Superstructure in Ultrahigh Speed Spun Fibers of Poly(Ethylene Terephthalate)

K. FUJIMOTO,* K. IOHARA, S. OHWAKI, and Y. MURASE

Fiber & Textile Research Laboratories, Teijin Ltd., 3-4-1, Minohara, Ibaraki-shi, Osaka, Japan

SYNOPSIS

Ultrahigh speed spinning of poly(ethylene terephthalate) (PET) was carried out at various take-up velocities from 5 to 10 km/min. The superstructure of as-spun fibers was characterized by small-angle X-ray scattering (SAXS), wide-angle X-ray diffraction (WAXD), viscoelastic properties, and scanning electron microscopy (SEM). Above 6 km/min the peaks or shoulders that are due to the interference between microfibrils appear on the equatorial SAXS intensity curves. The interfibrillar spacing estimated from the peak position increases with increasing take-up velocity. Comparison of the spacing with the lateral crystal sizes estimated from the broadness of the crystal ($hk0$) WAXD peaks indicates that the microfibril diameter becomes thick with increasing take-up velocity. Although the orientation and density in amorphous region for high-speed spun fibers are very low on the average, it can be seen that a few highly extended tie molecules exist in that region, and the number of these molecules increases with increasing take-up velocity. The modes and mechanisms of fibrillation induced by a rubbing test are discussed relating to these results.

INTRODUCTION

The structure and properties of PET fibers spun at high speed have been widely studied. According to those studies, crystallization takes place in the spin line at take-up velocities above 5 km/min, resulting in a high degree of orientation along the fiber axis.[1,2] The critical take-up velocity above which the crystallization takes place lowers with increasing spinning draft[3] and the molecular weight of the polymer.[4] The crystal size increases and the crystal lattice becomes more compact with take-up velocity.[2,5] On the other hand, the degree of molecular orientation in the amorphous region is much less in high-speed spun fibers than in conventional fibers produced by low-speed spinning and subsequent drawing, which is called FOY.[1,6] Ultrahigh speed spinning above 8 km/min results in a skin–core double structure.[6] The degrees of orientation and crystallinity are higher in the skin part than in the core.[6] Decreases in tenacity, birefringence, and crystal density of fibers spun at high take-up velocities are considered due to the formation of the skin–core structure.[5,6]

It is well known that a polymer has various superstructures[7] depending on the ways of processing. In order to clarify the structure of ultrahigh speed spun fibers, we must study the superstructures of various orders such as those of the crystalline–amorphous regions, fibril–microfibril, and skin–core. The structure of the crystalline region of high-speed spun fibers has been already analyzed in detail.[2,4,5] Relatively little is known, however, of the superstructures of higher orders, especially microfibrils, which are one of the most important structural elements of crystalline polymer solids.[8,9] In this article, the microfibrillar and the inner structure of as-spun PET fibers are studied mainly in relation to take-up velocity using X-ray diffraction, viscoelastic properties, and scanning electron microscopy (SEM).

* To whom all correspondence should be addressed.

Journal of Applied Polymer Science, Vol. 42, 1509–1517 (1991)
 CCC 0021-8995/91/061509-09$04.00

EXPERIMENTAL

Spinning

The PET polymer used in this study has an intrinsic viscosity of 0.64 and contains 0.3% TiO_2 by weight. Spinning experiments were carried out at a constant throughput rate of 6.2 g/min per orifice using a six-orifice spinneret. The diameter of each orifice was 0.3 mm. The take-up velocity was changed from 5 to 10 km/min.

Measurements

Wide-angle X-ray diffraction (WAXD) photographs were taken by a flat camera in a Rigaku Denki Ru-300 type apparatus. The WAXD intensity curves were measured using a Rigaku Denki PSPC (position-sensitive proportional counter) system. Nickel-filtered CuKα radiation was used throughout all these works. Apparent crystal sizes were estimated from the WAXD profiles of the (100), (010), and ($\bar{1}$05) reflections using Scherrer's equation.[10] The degree of crystal orientation f_c was obtained by

$$f_c = (180° - H)/180° \quad (1)$$

where H is the half-width of the intensity curve along the azimuth of the (100) reflection.

Small-angle X-ray scattering (SAXS) photographs and intensity curves were obtained using a Rigaku Denki Ru-300 type apparatus. The SAXS intensity was measured along the equator under the following collimating system: the first pinhole, 0.2 mm in diameter, and the second pinhole, 0.15 mm, were put before a specimen, and the PSPC was set behind the specimen through a vacuum path. The slit, 1.0 mm in height, was set in front of the PSPC probe in order to detect the only equatorial scattering.

The distribution of refractive indices parallel and perpendicular to the fiber axis ($n_{\parallel}$ and $n_{\perp}$) along the radius of fibers were measured using a Interphako interference microscope (Carl Zeiss Jena) and were calculated by Kuhnle's method.[6] Birefringence was obtained as $\Delta n = n_{\parallel} - n_{\perp}$. The scanning electron microscopic (SEM) observation was carried out using a JSM-840 (JEOL), in which sample fibers were coated with gold.

Dynamic viscoelastic properties were measured as a function of temperature using a Iwamoto spectrometer. The frequency was 10 Hz and the heating rate was 3°C/min. Density was measured using a density gradient column with a mixture of n-heptane–tetrachloromethane. The infrared absorption spectra were measured by the KBr method with a FT-IR III (Japan Spectroscopic Co.). The melting behavior was measured in the fixed and unfixed states at a constant heating rate of 10°C/min using a Rigaku Denki DSC-10A differential scanning calorimeter (DSC), in which the fibers were fixed by winding around the lid of sample pan.

RESULTS AND DISCUSSION

Skin–Core Structure

Figure 1 shows the radial distribution of birefringence of fibers spun at various take-up velocities from 5 to 10 km/min. The difference of birefringence between the center (core) and surface (skin) is small, up to 8 km/min. However, the birefringence of the core part becomes extremely low above 9 km/min, although that of the skin part is kept at a high level. Thus the well-known skin–core double structure is formed in the ultrahigh speed spun fibers.

Figure 2 shows the DSC thermograms measured in fixed and unfixed states for fibers spun at various take-up velocities. The endotherm is observed near 255°C at take-up velocity of 5 km/min. This is considered due to the melting of the crystal formed during the DSC measurement, because the WAXD pattern of these fibers shows only an amorphous halo (as shown later in Fig. 9). The exotherm due to crystallization is observed at about 100°C. This exotherm cannot be observed for the fibers spun at 7 km/min, because the crystallization already takes place in the spinline. However, the exotherm of

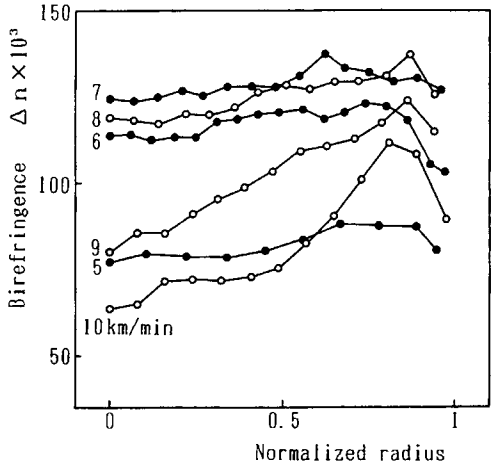

Figure 1 Birefringence distributions in cross sections of PET fibers spun at various take-up velocities.

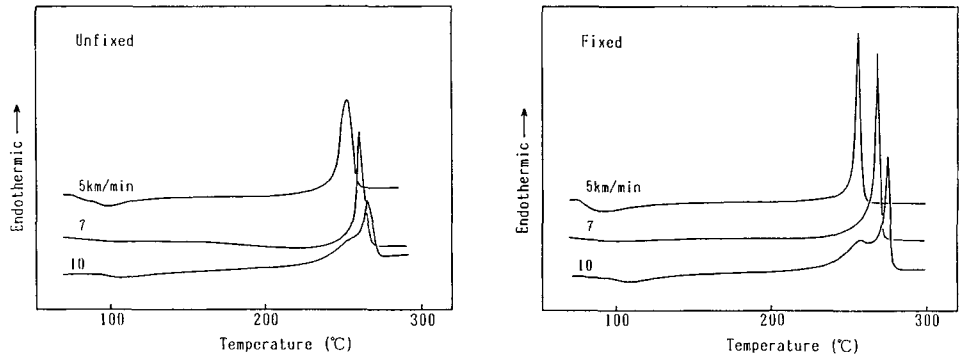

Figure 2 Change of DSC thermograms measured in the fixed and unfixed states with take-up velocity.

crystallization appears again above 9 km/min, and the melting endotherm splits into two peaks. These exothermic and lower endothermic peaks approximately agree with those of 4–5 km/min fibers. This implies that the structure of the core part spun above 9 km/min is similar to that of 4–5 km/min fibers in which crystal is not formed.

Microfibril Structure

Figure 3 shows SAXS photographs of as-spun fibers obtained at various take-up velocities. In the case of 5 km/min, the equatorial streak appears without any other scatterings being observed. In addition to this equatorial streak, the X-shaped scattering appears at 6 and 7 km/min fibers. Above 8 km/min, the X-shaped scattering disappears and the diffuse two-spot pattern appears on the meridian, as already reported by Shimizu et al.[6]

Figure 4 shows the change in equatorial SAXS intensity curves with take-up velocity. The scattering intensity at 5 km/min decreases monotonously with scattering angle, while peaks or shoulders appear above 6 km/min. The equatorial diffuse streak

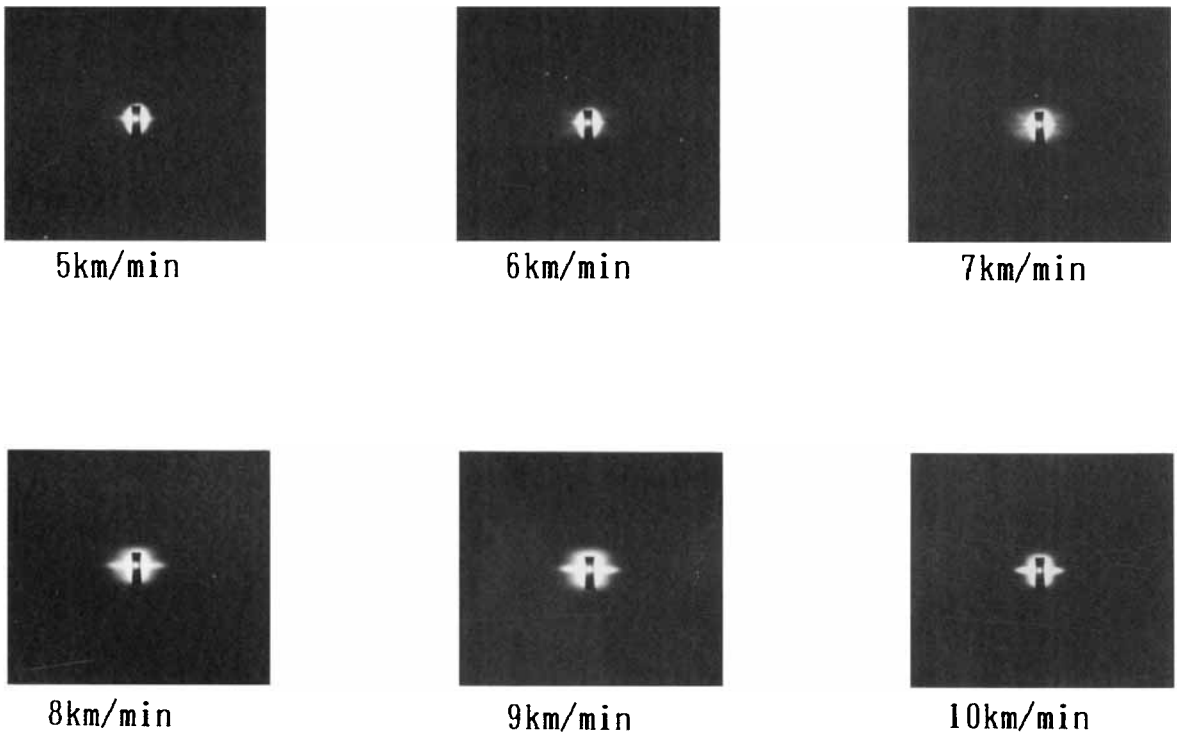

Figure 3 Small-angle X-ray scattering photographs of PET fibers spun at various take-up velocities.

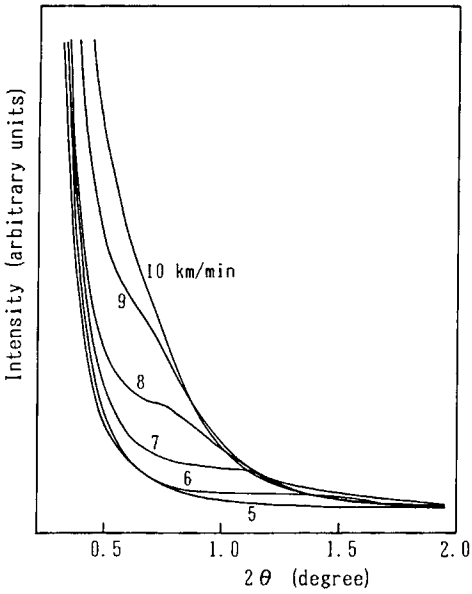

Figure 4 Equatorial SAXS intensity curves of PET fibers spun at various take-up velocities.

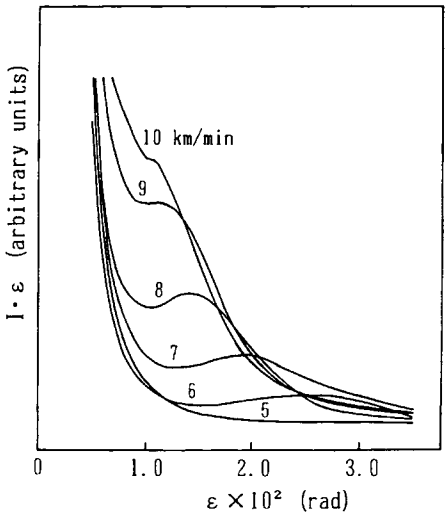

Figure 5 Corrected equatorial SAXS intensity curves $[I(\chi)\chi - \chi]$ of PET fibers spun at various take-up velocities: I, intensity; χ, scattering angle.

is often observed in SAXS patterns of polymers, especially fibers, because of the microfibrils of nonuniform diameter.[11] However, an equatorial interference peak appears in some rare cases such as regenerated cellulose[12] and poly(4-methyl-1-pentene).[13] It should be noted that this rare phenomenon occurred in our PET fibers spun at high take-up velocities.

The peak or shoulder shifts to the lower scattering angle with increasing take-up velocity and becomes indistinct above 9 km/min due to the effect of central scattering. Figure 5 shows the relation of $I(\chi)\chi - \chi$, where $I(\chi)$ is the SAXS intensity at a scattering angle χ. Since in this case the X-ray scattering is concentrated on the equator, the $I(\chi)\chi - \chi$ plot was adopted instead of the $I(\chi)\chi^2 - \chi$ plot for isotropic scattering.[14] The existence of a shoulder above 9 km/min is confirmed by Figure 5. These results indicate that the PET fibers spun above 6 km/min consist of microfibrils of almost uniform diameter orienting parallel to the fiber direction. Since such microfibrils as these have not been reported for conventional spun and drawn PET fibers, it can be seen that this microfibrillar structure of this nature is characteristic to the fibers spun at high take-up velocities.

Figure 6 shows the interfibrillar spacing calculated from the peak angles using Bragg's law. Thus, estimated spacings are 60 Å at 6 km/min and 145 Å at 10 km/min: the interfibrillar spacing increases with take-up velocity. In the following section, the crystal size estimated from WAXD profiles will be shown to follow the same tendency as that of SAXS. This suggests that just one crystal is contained in the cross section of a microfibril and that the increase of the interfibrillar spacing is attributed to the increase of the microfibril diameter. The equatorial SAXS intensity increases with take-up velocity, as seen in Figure 4. This may be due to the increase in the difference of electron densities between the inside of microfibril and the interface region between microfibrils, in particular the decrease of electron densities in the interface region.

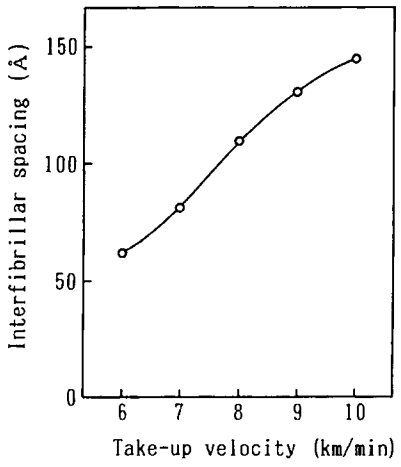

Figure 6 Change of interfibrillar spacing with take-up velocity.

Figure 7 shows the SEM photographs of the fibers treated with a NaOH aqueous solution at room temperature. In this figure, large pores are due to the dispersion of TiO_2 particles on the fiber surfaces, and the microfibrillar structure cannot be observed directly, except for many lines along the fiber axis,

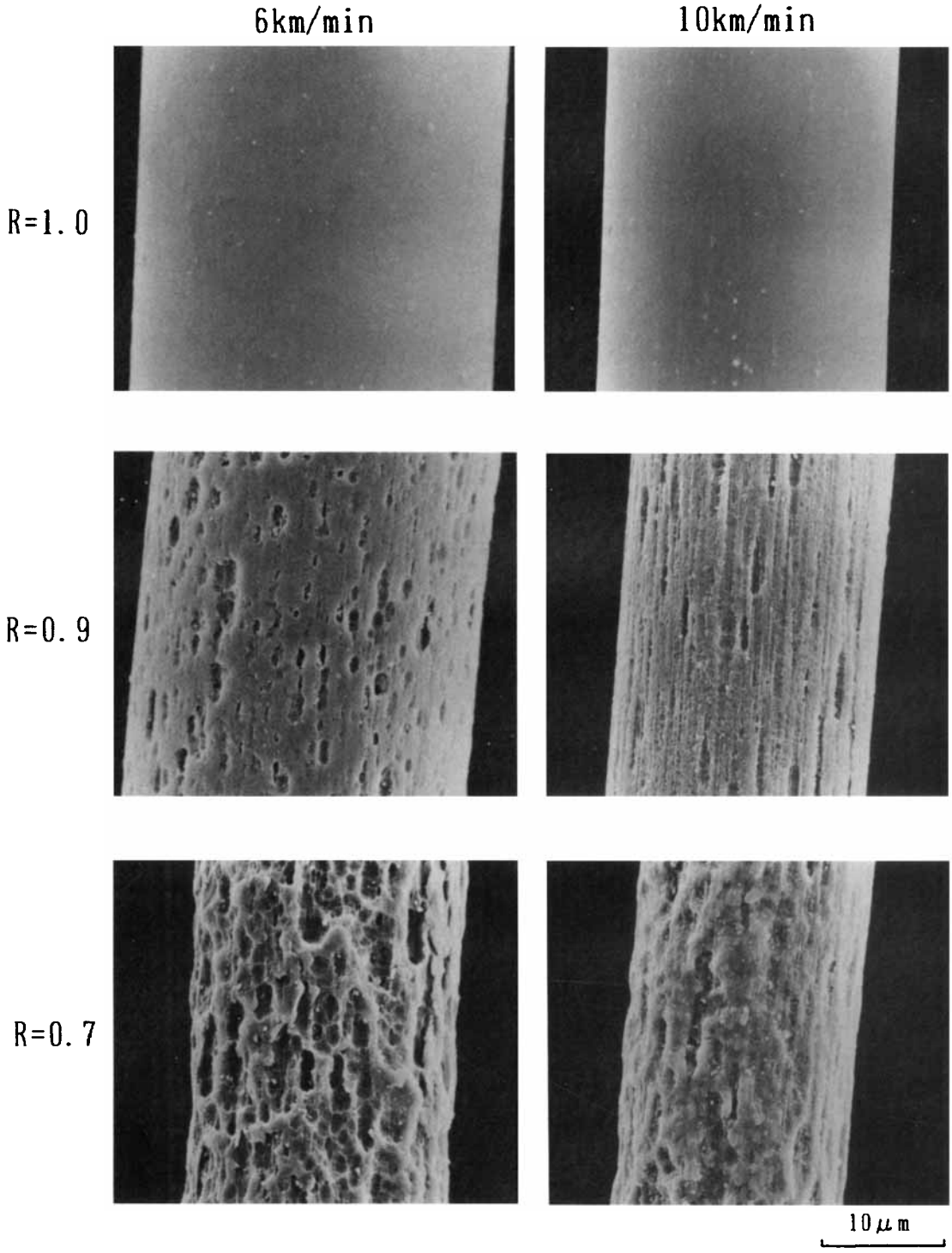

Figure 7 Change in SEM photographs of PET fibers treated with NaOH solution at room temperature. Numbers on the photographs indicate radius of fibers after alkali treatment.

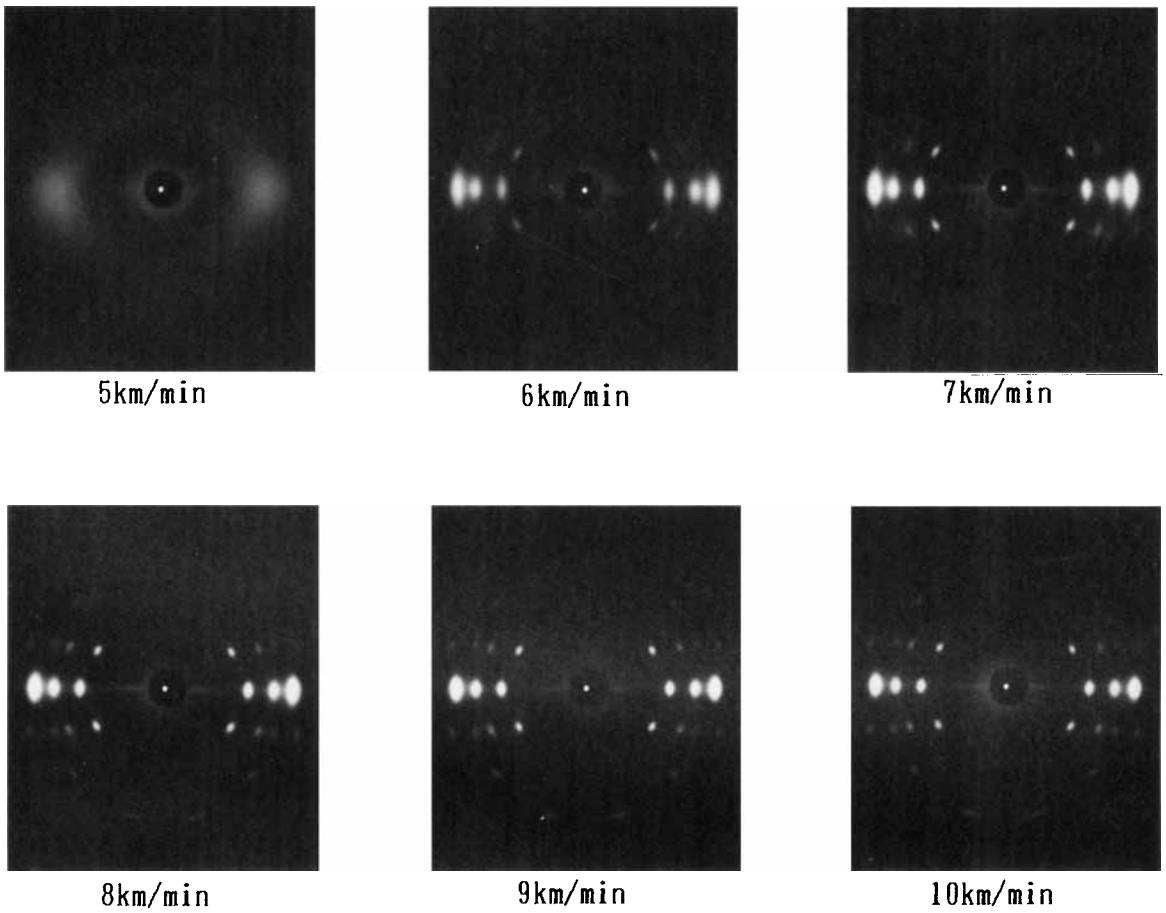

Figure 8 Wide-angle X-ray diffraction photographs of PET fibers spun at various take-up velocities.

especially for 10 km/min fibers. These lines suggest that microfibrils are formed even at the relatively inner part of fibers when being spun at ultrahigh take-up velocities.

Structure of Crystalline Region

Figure 8 shows WAXD photographs of as-spun fibers obtained at various take-up velocities. An amorphous halo tends to concentrate toward the equator at 5 km/min, indicating that molecular chains orient along the fiber axis without any distinct crystallization. Above 6 km/min, the crystalline reflections become sharp both along the equator and azimuth with increasing take-up velocity. Table I shows the apparent crystal sizes, the lattice spacings, and the degree of crystal orientation. The symbol L_{hkl} stands for the crystal size perpendicular to the (hkl) plane; d_{hkl} stands for the (hkl) lattice spacing. The values of L_{100} and L_{010} increase mono-

Table I Crystal Sizes, Lattice Spacings, and Degree of Crystal Orientation for PET Fibers Spun at Various Take-up Velocities

Take-up Velocity (km/min)	L_{100}	L_{010}	$L_{\bar{1}05}$	d_{100}	d_{010}	$d_{\bar{1}05}$	f_c (%)
6	50 Å	61 Å	51 Å	3.437 Å	5.072 Å	2.100 Å	92
7	75	86	70	3.425	5.042	2.099	94
8	98	94	89	3.413	5.020	2.098	94
9	108	99	97	3.402	5.013	2.098	95
10	112	100	101	3.396	4.991	2.098	95

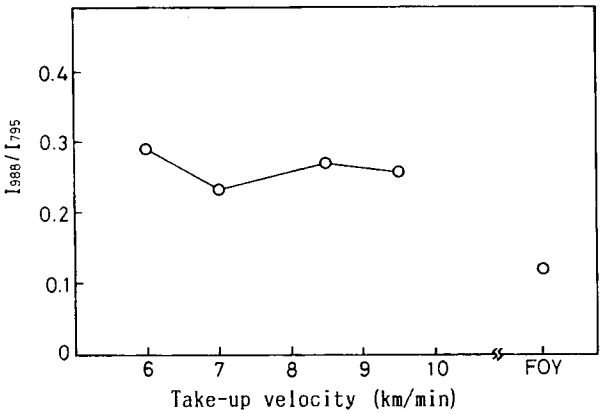

Figure 9 Change of absorption ratio (988 cm^{-1}/795 cm^{-1}) with take-up velocity.

tonically with take-up velocity, and interestingly, the increase of L_{100} is more remarkable than that of L_{010} at the higher take-up velocities.[2,5] It has been recognized that L_{100} develops selectively in the fibers quenched at the initial stage of crystallization along the spin line.[15] The crystal size L_{100} is that in the a-axis direction, along which aromatic rings are stacked due to π-electron interaction between them.[2] The $L_{\bar{1}05}$, reflecting the sizes along the c (chain) axis, also increases with take-up velocity but tends to level off above 8 km/min. The d_{100} and d_{010} spacings decrease with take-up velocity, but the $d_{\bar{1}05}$ does not change so much as these two. This means that the crystals formed during high-speed spinning have a compact lattice, especially perpendicular to the fiber axis. The degree of crystal orientation is shown already at a high level at 6 km/min fibers and increases slightly with take-up velocity.

Figure 9 shows the change of infrared absorption ratio I_{988}/I_{795} with take-up velocity. The 988 cm^{-1} band attributed to the molecules folded on the crystal surface[16] is stronger in fibers spun above 6 km/min than in FOY. The crystallization takes place during high-speed spinning, resulting in a larger number of chain folding compared with that of FOY and, in other wards, a crystal of lamellar type. It is well known that high-speed spun isotactic-polypropylene (itPP) fibers show a remarkable hard elasticity[17] characterized by the particularly high extensibility and strain recoverability.[18] In this case of PET fiber, however, no high hard elasticity is

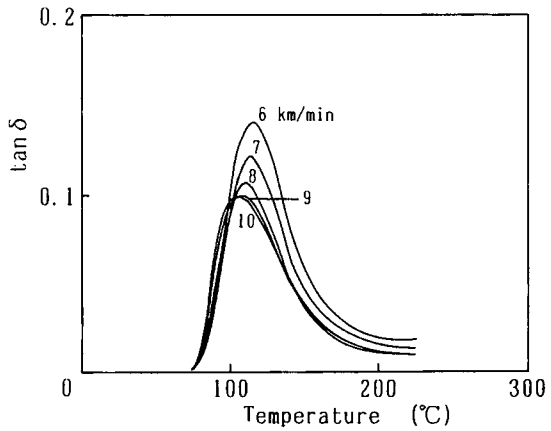

Figure 10 Temperature dependence of mechanical tan δ for PET fibers spun at various take-up velocities.

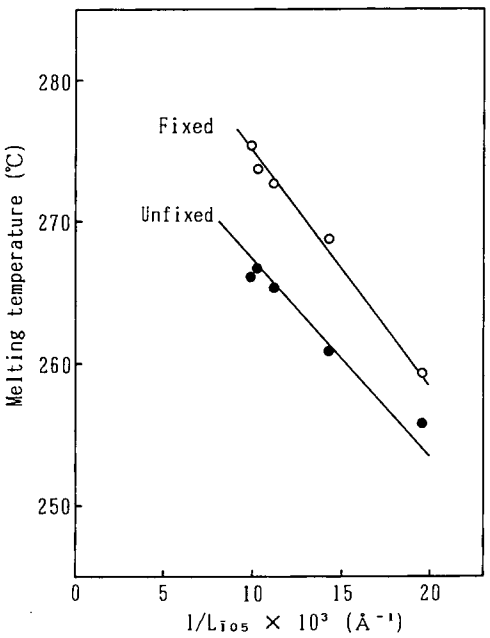

Figure 11 Change of melting temperature measured in the fixed and unfixed states with reciprocal of crystal thickness ($L_{\bar{1}05}$) for PET fibers.

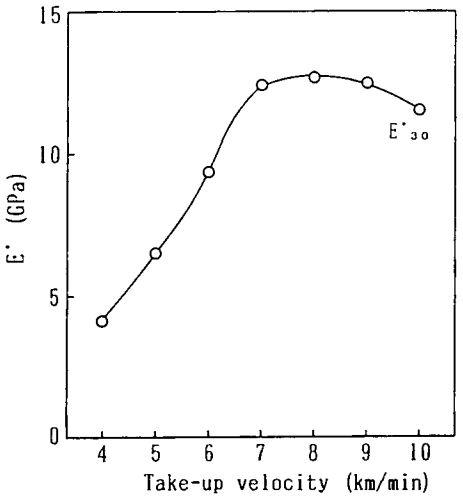

Figure 12 Mechanical storage modulus at 30°C of PET fibers spun at various take-up velocities.

achieved because of its larger number of tie molecules connecting adjacent lamellae than in itPP.

Structure of Amorphous Region

Figure 10 shows the dynamic loss tangent (tan δ)–temperature curves. It is recognized that the α dispersion is related to the thermal micro-Brownian motion of armorphous chains.[19] The peak temperature of tan δ decreases with increasing take-up velocity. This suggests that the molecular orientation and/or density in the amorphous region lowers with take-up velocity, as already reported in many studies.[1,6]

However, the existence of relatively high extended tie molecules will be suggested from the following two results: Figure 11 shows the change of melting temperature measured in the fixed and unfixed state with the reciprocal of the crystal thickness ($L_{\bar{1}05}$) for fibers spun at various take-up velocities. Since this plot in the unfixed state shows approximately linear relation and the value at $1/L_{\bar{1}05} \rightarrow 0$ is close to the equilibrium melting temperature,[20] the rise in the melting temperature may be explained by the increase of the crystal thickness. In the fixed state the melting temperature is always higher than that in the unfixed state at the same crystal thickness. This increase is considered due to the superheating caused by the orientation of the amorphous molecules. Moreover, the difference in the melting temperature between the fixed and the unfixed state increases with increasing take-up velocity. This means that relatively highly extended tie molecules exist in the amorphous region, and the number of these molecules increases with increasing take-up velocity. Figure 12 shows the change of storage dynamic modulus measured at 30°C (E'_{30}) with take-up velocity. This velocity E'_{30} increases up to 8 km/min and then slightly decreases. Considering that the skin–core structure is formed and the molecular orientation in the amorphous region becomes very low at ultrahigh take-up velocities, the decrease of E'_{30} is supposed to be too small. The existence of the highly extended tie molecules is also supported from this result. Summarizing the preceding results, although the degree of molecular orientation in the amorphous region is very low on the average for high-speed spun fibers, a few highly extended tie molecules exist in that region.

Macrofibril

Figure 13 shows SEM photographs of fibers subjected to the rubbing test, which was carried out

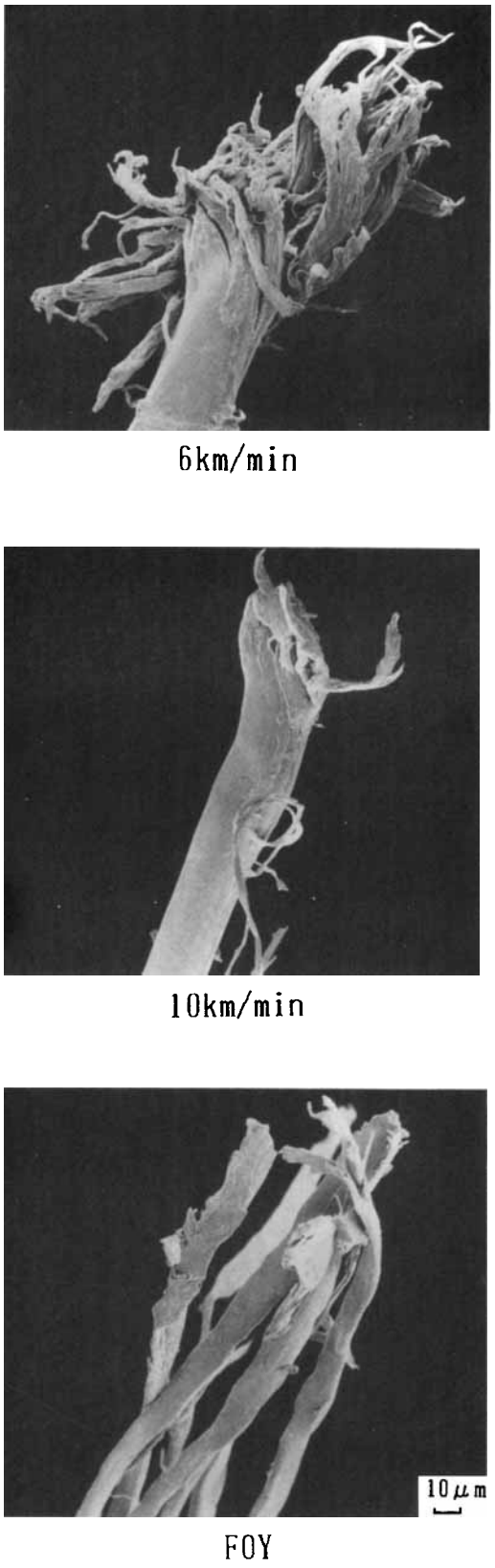

Figure 13 SEM photographs of broken surfaces of PET fibers subjected to rubbing test.

according to JIS-L-0823, where fibers were rubbed with dry cloth. The broken surface of FOY consists of several split, long and thick fibrils (macrofibrils); while in the case of 6 km/min many short and thin fibrils appear. It is interesting to note that the broken surface of fiber spun at 10 km/min shows a morphology indicating melting destruction rather than that due to fibrillation.

Since microfibril diameter is not uniform in the case of FOY, during the rubbing test the shear stress may concentrate at a few points where the cohesive force between the microfibrils is relatively weak. On the other hand, in the case of fibers spun at as high speed as 6 km/min, the shear stress is uniformly applied on the surface because of the uniformity of the microfibril diameter, resulting in many fine fibrils. In the case of fibers spun at ultrahigh speeds such as 10 km/min, which have a skin–core double structure, the shear stress may cause the destruction of the core part with low degrees of molecular orientation and crystallinity, resulting in the morphology of melting destruction.

The authors wish to thank Professor Miyasaka of the Tokyo Institute of Technology for his helpful advice and discussions.

REFERENCES

1. J. Shimizu, K. Toriumi, and K. Tamai, *J. Soc. Fiber Sci. & Tech., Jpn. (Sen-i Gakkaishi),* **33,** T-208 (1977).
2. H. M. Heuvel and R. Huismann, *J. Appl. Polym. Sci.,* **22,** 2229 (1978).
3. J. Shimizu, N. Okui, A. Kaneko, and K. Toriumi, *J. Soc. Fiber Sci. & Tech., Jpn. (Sen-i Gakkaishi),* **34,** T-64 (1978).
4. J. Shimizu, N. Okui, T. Kikutani, and K. Toriumi, *J. Soc. Fiber Sci. & Tech., Jpn. (Sen-i Gakkaishi),* **34,** T-93 (1978).
5. J. Shimizu, T. Kikutani, A. Takaku, and N. Okui, *J. Soc. Fiber Sci. & Tech., Jpn. (Sen-i Gakkaishi),* **40,** T-63 (1984).
6. J. Shimizu, N. Okui, and T. Kikutani, *J. Soc. Fiber Sci. & Tech., Jpn. (Sen-i Gakkaishi),* **37,** T-135 (1981).
7. S. Manabe, *Kobunshi no Kotaikozo II,* S. Kanbara, Ed., Kyoritu, Tokyo, 1984, p. 489.
8. K. Miyasaka, *Kobunshi High Polymers, Jpn.,* **36,** 350 (1987).
9. K. Miyasaka, *J. Soc. Fiber Sci. & Tech., Jpn. (Sen-i Gakkaishi),* **43,** 119 (1987).
10. L. E. Alexander, *X-Ray Diffraction Methods in Polymer Science,* Wiley, New York, 1969.
11. R. Bonart and R. Hosemann, *Kolloid-Z., Z. Polymere,* **186,** 16 (1962).
12. P. H. Hermans and A. Weidinger, *J. Polym. Sci.,* **14,** 397 (1950).
13. T. Tanigami, K. Yamaura, S. Matsuzawa, K. Ohsawa, and K. Miyasaka, *J. Appl. Polym. Sci.,* **32,** 4491 (1986).
14. M. Kakudo, *Xsen Kesshogaku,* I. Nita, Ed., Maruzen, Tokyo, 1961, p. 517.
15. K. Fujimoto, K. Iohara, S. Ohwaki, and Y. Murase, *J. Soc. Fiber Sci. & Tech., Jpn. (Sen-i Gakkaishi),* **44,** 171 (1988).
16. J. L. Koenig and J. M. Honnon, *J. Macromol. Sci.,* **B1,** 199 (1967).
17. Y. Shimizu, H. Akabane, A. Tanioka, K. Miyasaka, and K. Ishikawa, *J. Polym. Sci. Phys. Ed.,* **17,** 1495 (1979).
18. J. Shimizu, N. Okui, and T. Kikutani, *J. Soc. Fiber Sci. & Tech., Jpn. (Sen-i Gakkaishi),* **36,** T-166 (1980).
19. M. Takayanagi, *J. Polym. Sci.,* **61,** S7 (1962).
20. A. Mehta, U. Gaur, and B. Wunderlich, *J. Polym. Sci. Phys. Ed.,* **16,** 289 (1978).

Accepted July 7, 1990